Medical Devices: Evidence and Research

Dovepress
open access to scientific and medical research

Open Access Full Text Article

CASE REPORT

# Cerebrovascular Responses in a Patient with Lundberg B Waves Following Subarachnoid Haemorrhage Assessed with a Novel Non-Invasive Brain Pulse Monitor: A Case Report

Elliot John Teo[1,2], Sigrid Petautschnig[1,2], Jack Hellerstedt[1], Sally A Grace[1], Jacqui S Savage[1], Brendan Fafiani[1], Paul Daniel Smith[3,4], Ashu Jhamb[5], Timothy Haydon[2,6], Barry Dixon[1,5,6]

[1]Cyban Pty Ltd, Melbourne, Victoria, Australia; [2]Department of Critical Care Medicine, St Vincent's Hospital, Melbourne, Victoria, Australia; [3]Department of Neurosurgery, St Vincent's Hospital, Melbourne, Victoria, Australia; [4]University of Melbourne Medical School, Melbourne, VIC, Australia; [5]Department of Medical Imaging, St Vincent's Hospital, Melbourne, Victoria, Australia; [6]Department of Critical Care, the University of Melbourne, Melbourne, VIC, Australia

Correspondence: Barry Dixon, Department of Critical Care Medicine, St Vincent's Hospital (Melbourne), 41 Victoria Parade, Fitzroy, VIC, 3065, Australia, Tel +61 439 618 815; +61 3 9231 4425, Email barry.dixon@cyban.com.au

**Abstract:** Subarachnoid haemorrhage (SAH) can trigger a range of poorly understood cerebrovascular responses that may play a role in delayed cerebral ischemia. The brain pulse monitor is a novel non-invasive device that detects a brain photoplethysmography signal that provides information on intracranial pressure (ICP), compliance, blood flow and tissue oxygen saturation. We monitored the cerebrovascular responses in a patient with Lundberg B waves following a SAH. The patient presented with a Fischer grade 4 SAH that required urgent left posterior communicating artery aneurysm coiling and ventricular drain insertion. On hospital day 4 oscillations or spikes on the invasive ICP were noted, consistent with Lundberg B waves. Brain pulse monitoring demonstrated concurrent pulse waveform features consistent with reduced brain compliance and raised ICP over both brain hemispheres. Oxygen levels also demonstrated slow oscillations correlated with the ICP spikes. Brief infrequent episodes of reduced and absent brain pulses were also noted over the right hemisphere. Our findings suggest that the brain pulse monitor holds promise for early detection of delayed cerebral ischemia and could offer insights into the vascular mechanisms at play.

**Plain Language Summary:** In this study, we examined a patient with a serious brain bleed, known as subarachnoid hemorrhage (SAH). Patients with SAH can suffer from vasospasm and consequent delayed cerebral ischemia (DCI), which can happen from 4 to 14 days after the initial bleeding. Detecting and treating DCI early is difficult because methods are imperfect, discontinuous and technically difficult.

We used a new, non-invasive device that can monitor various features of brain health. This device helps us understand the pressure inside the skull, blood flow, and the oxygen saturation on the surface of the brain. In this patient, we found evidence of:

- Brain pulse signals that were directly related to acute changes in the invasive intracranial pressure.
- Specific brain pulse patterns that may indicate a local reduction in brain blood flow.
- Signs of a breakdown in the brain's ability to regulate blood flow in the injured hemisphere.
- The oxygen saturation levels in the brain that related to pressure changes.

These results are promising because they suggest the new device could help us identify when someone's brain condition is getting worse. This ability could guide the development of improved care protocols, and aid clinical decision-making. Further research is needed in this patient population with additional forms of monitoring to understand the generalizability of our findings.

**Keywords:** near infra-red, spreading depolarisation, vasoconstriction, intracranial pressure, brain compliance, brain oxygen



Received: 19 December 2023
Accepted: 9 February 2024
Published: 19 February 2024

## Introduction

Subarachnoid haemorrhage (SAH) may be complicated by delayed cerebral ischemia (DCI) that peaks 4 to 14 days following the initial bleed. The cerebrovascular responses associated with DCI remain poorly understood but include large vessel vasospasm of arteries, veins, microvascular vasoconstriction, microvascular thrombosis, and hyper-perfusion.[1–7] Early detection and treatment of DCI remains a challenge due to limitations in the monitoring methods, uncertainty in the pathogenesis and lack of compelling evidence supporting treatments, such as spasmolysis.[8,9] In patients with impaired conscious states, monitoring largely relies on clinical neurological examination, which often results in delayed recognition of deterioration, increasing the risk of adverse outcomes.[10–12]

The onset of DCI is associated with ICP variability.[13] One canonical example of ICP variation is Lundberg B waves, typically defined as brief repeating spikes in ICP (10–20 mmHg) with a frequency of 0.5–3 waves/min.[14] They are seen in a range of brain injuries and may be present normally in sleep.[15] Within the context of SAH, the presence of Lundberg B-waves has been recognized as a potential marker for intact cerebral autoregulation and is correlated with a good clinical outcome.[16] Studies using transcranial Doppler ultrasound found Lundberg B waves arise from brief periods of increased middle cerebral artery blood flow due to vasodilation in both SAH and TBI.[14,17–20] Lundberg B waves have also been associated with increased delta wave electroencephalogram (EEG) activity indicating a central mechanism and may play a role in the circulation of glymphatics.[21]

Continuous non-invasive brain pulse monitoring could provide earlier detection of deterioration and provide insights into the underlying mechanisms of injury, which could improve patient outcomes. The PPG signal provides information on intracranial pressure (ICP), compliance, blood flow and tissue oxygen saturation ($StO_2$).[22–24] Here we present a case demonstrating the monitor's ability to detect variations in the brain photoplethysmography (PPG) signal indicative of intracranial pressure fluctuations, compliance alterations, blood flow changes and tissue oxygen saturation ($StO_2$) in real-time, and non-invasively.

## Materials and Methods

### Brain Pulse Monitor

The monitor has been described in detail previously.[22–24] In brief, the monitor uses near-infrared (NIR) light sources (660 and 940 nm). Each brain sensor has a single light-emitting diode (LED) and photodetector (PD). The novel geometry of the LED and PD in the sensor housing preferentially detects photons reflected from the brain, minimizing extra-cranial contributions to the PPG signal. The sensors are placed on the temples over the left and right middle cerebral artery (MCA) territories and secured in position with a headband (Figure 1A).

### Optical Intensity and Brain Pulse Waveform

The optical intensity and brain pulse waveform PPG signals are analogous to those found with traditional skin pulse oximetry.[25] Under normal measurement conditions, the optical intensity is inversely proportional to the volume of light-absorbing substances within the illuminated area. Changes in measured intensity are therefore typically due to a change in blood distribution in the brain.[26,27]

The brain pulse waveform represents the relatively small amplitude cardiac pulsatile component of the optical signal. The underlying source of the brain pulse signal reflects cardiac-associated blood volume changes in the pial veins and venules within the subarachnoid space. The pial veins and venules are thin-walled, low-pressure vessels that have a relatively higher blood volume than arterioles or capillaries. An increase in ICP can compress and empty the pial venous system thus reducing the blood volume, while a reduction in ICP can reduce venous pressure and increase venous blood volume.[28–31] The PPG signal is feature-rich and allows estimation of blood flow, ICP, compliance and oxygen saturation.[22–24]

### Invasive ICP

An extra-ventricular drain was placed in the right lateral ventricle. The pressure levels were zeroed at the tragus and monitored by a Philips IntelliVue system. The physiological ICP waveforms were exported using ICM+ (Cambridge Enterprise, Cambridge, UK) for offline analysis.

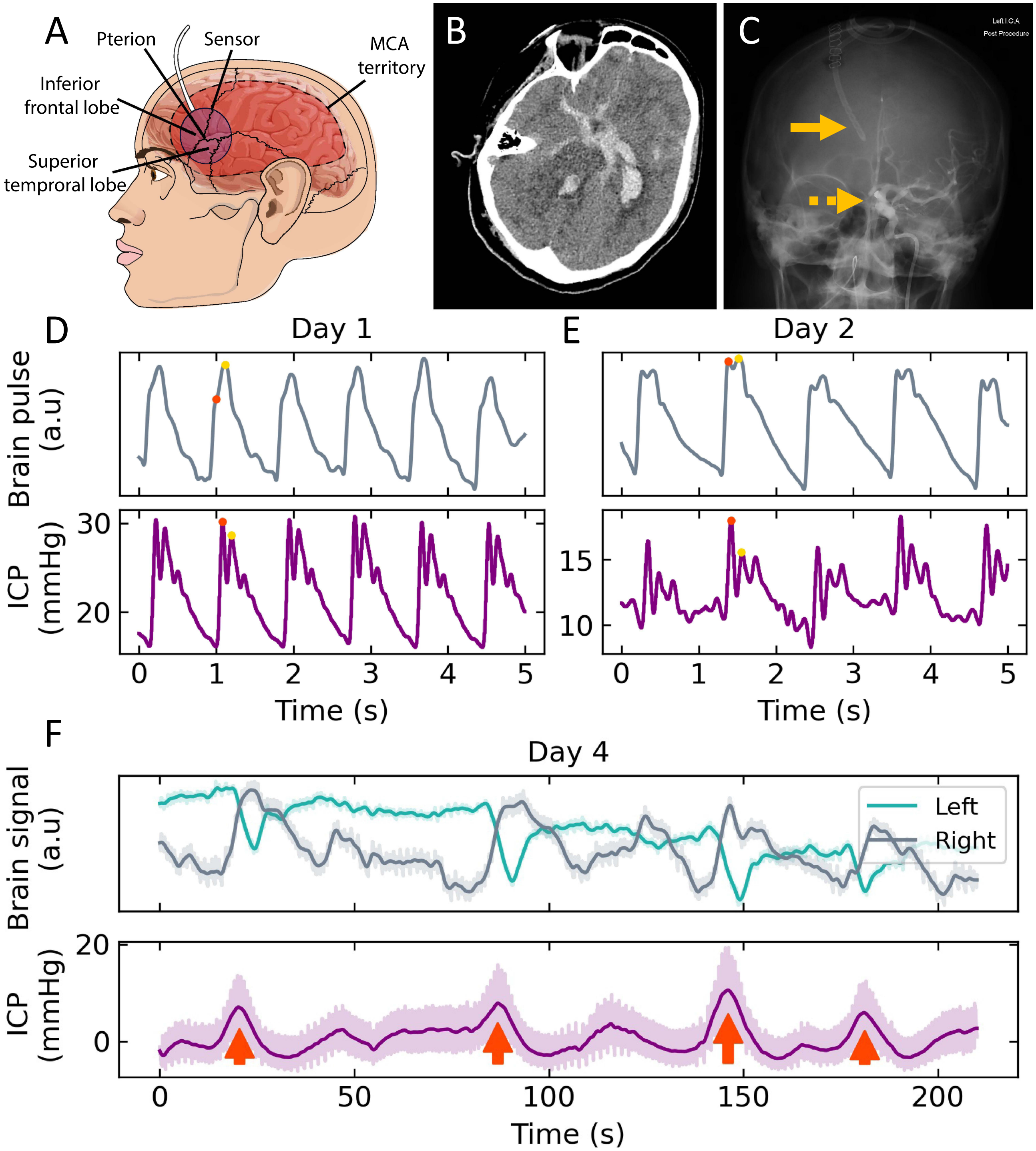


**Figure 1** (**A**) Headband placement of sensor over the temple and the relationship to the pterion, brain lobes and middle cerebral artery territory. (**B**) CT of grade 4 subarachnoid haemorrhage with blood in the basal cisterns, sylvian fissures, fourth and left lateral ventricles. (**C**) Percutaneous cerebral angiogram demonstrating right lateral ventricular drain (continuous arrow) and radio opaque coil securing the left posterior communicating artery aneurysm (dashed arrow). Comparison of brain pulse monitor and invasive ICP pulse waveforms on (**D**) Days 1 and (**E**) Day 2 following SAH. The ICP was higher on Day 1 and associated with a relatively higher P2 amplitude (yellow dot) to P1 (red dot) for both the invasive ICP and non-invasive pulse waveforms. On Day 2 the ICP was lower and the P2 to P1 relative amplitudes were also lower. (**F**) The brain pulse monitor optical intensity (upper panel) of the left and right brain hemispheres and invasive intracranial pressure (lower panel) demonstrating Lundberg B waves (red arrows).

**Abbreviations**: a.u, arbitrary units; MCA, middle cerebral artery; mmHg, millimetres of mercury; s, seconds.

## Signal Processing

The data acquired from the brain pulse monitor was recorded and saved for offline analysis. The sampling rate used for data acquisition was 500 Hz. Data processing and analysis was performed using scientific computing packages written in the Python programming language.[32,33] Where indicated, either a low-pass filter with a cut-off frequency of 0.5 Hz was applied, or a Butterworth bandpass filter was applied, with cut-off frequencies of 0.5 Hz and 8.5 Hz. Continuous wavelet decomposition (CWT) was performed on the bandpass-filtered signal using the Morlet wavelet, to estimate the power of the cardiac component from the frequency domain. Fixed intensity contour lines were added for visualization purposes.

The sum of power intensity of the CWT transform in the [1, 1.5] Hz region was used to assess reductions of brain signal pulsatility; periods of reduced power relative to the median value (one standard deviation) were defined as "poor pulsatility signal".

## ICP

The brain pulse waveform shares morphological features with the invasive ICP waveform. The normal ICP waveform is usually comprised of 3 peaks: P1 (the percussion wave, representing the early systolic arterial pulse), P2 (the mid/late systolic reflected tidal wave associated with intracranial volume changes) and P3 (a second late reflected wave or diastolic arterial pulse).[28] Normal ICP levels are associated with the relative amplitudes of the peaks, where P1 > P2 > P3. With raised ICP and reduced brain compliance there is an increase in the amplitude of P2 and P3 relative to P1. One method to estimate the ICP and compliance is to calculate the amplitude of the P2 component relative to P1.[34] Raised ICP and reduced compliance are also associated with a longer time to the pulse peak (TTP).[35,36]

To assess the morphological features associated with raised ICP and compliance, we determined the amplitude of the pulse at 45% (early diastole) relative to 10% (early systole) of the pulse period: the "DS ratio". This straightforward feature extraction provides a comparable value to the P2/P1 ratio. We also extracted the TTP per cardiac cycle.

## Brain Tissue Oxygen Saturation ($StO_{2\%}$)

To quantify the quality of the brain signal, the energy of the two dominant frequency components is compared to the sum of remaining components from a spectral decomposition process in an 8-second window.[37,38] If the dominant two frequencies are less than the rest, it indicates that higher frequency components such as noise or non-pulsatile elements are overpowering the main heart rate frequency, in which case the signal is no longer considered pulsatile and therefore is unsuitable for $StO_2$% estimation. A proprietary algorithm has been developed based on feature extraction from a modified ratio-of-ratios approach[25] to calculate a calibrated $StO_2$% estimation from the recorded signal.

## Statistical Analysis

To quantitatively compare the DS ratio, TTP, and $StO_2$ values extracted from the brain signal recordings to the invasive ICP measurements, linear least-squares regression was performed for a variety of subsets of data as explained in the Results section. Coefficients of determination $R^2$ and p-values were reported from the results of this fitting.

# Results

## Patient Characteristics

A 52-year-old woman was admitted to hospital after developing an intense acute left-sided headache with reduced conscious state. A brain computed tomography (CT) scan demonstrated a SAH (Modified Fisher Grade 4) with extensive blood in the basal cisterns, sylvian fissures and ventricles, but predominately in the left lateral ventricle. Early hydrocephalus was present. A computed tomography angiogram (CTA) demonstrated a left posterior communicated artery aneurysm, shown in Figure 1B.

The patient required intubation and underwent a percutaneous coiling of the aneurysm with insertion of a ventricular drain into the right lateral ventricle that provided invasive intracranial pressure monitoring (Figure 1C). She was admitted to the ICU and commenced on regular nimodipine.

Examples of waveform morphologies on hospital days 1 and 2 measured simultaneously by the invasive ICP monitor and the brain pulse monitor are shown in (Figure 1D and E).

The patient was extubated on the third hospital day. Her Glasgow coma score (GCS) fluctuated from 11 to 14. She had weakness in her right arm and leg 2/5 and was agitated at times. Her Richmond agitation sedation scale (RASS) ranged from −1 to +2, requiring restraints and sedatives intermittently. A CTA on this day did not demonstrate evidence of large vessel vasospasm.

On the fourth hospital day, the invasive monitoring demonstrated ICP spikes consistent with Lundberg B waves. The ICP peak oscillated between 5 and 20 mmHg, at a frequency of ~3 per minute.[14] The Lundberg B wave morphology was symmetrical in shape (Figure 1F, lower panel). The heart rate was stable around 70 beats per minute. On examination, the patient appeared fatigued but rousable with a RASS of −1; the GCS ranged from 13 to 14 and neurological findings were consistent with the previous day. A CTA the next day did not demonstrate evidence of large vessel vasospasm.

The patient was discharged to the ward on hospital day 5. Subsequently, a ventriculo-peritoneal shunt was required for ongoing hydrocephalus. The patient was discharged home after 38 days in hospital, with some limitations of memory and executive function and mild right-sided weakness.

## Brain Pulse Monitoring of Lundberg B Waves, ICP and Compliance

Slow oscillations of the optical intensity were observed in both brain hemispheres synchronous with the Lundberg B waves (Figure 1F, upper panel). Sharp decreases in left-side intensity were accompanied by broad increases in the right. Our subsequent analysis focused on the four dominant Lundberg B waves indicated by red arrows in Figure 1F lower panel where these corresponding optical changes were observed.

Single pulses for one such event are plotted in Figure 2. Over the 6 to 8 brain pulses associated with the Lundberg B wave ICP spike, the brain pulse waveforms (in both hemispheres) demonstrated comparable morphological changes. We focused on two specific features: First, the early diastolic to early systolic amplitudes ratio (DS ratio), and second, the time elapsed from the preceding trough, to signal maximum in the cardiac cycle ("Time to pulse peak", TTP). These are explicitly labelled for the four single peaks plotted in the lower panels (A–D) in Figure 2. For these purposes, we took the early diastolic (systolic) to be at 45% (10%) time elapsed fractions of the cardiac cycle.

The panels A–D were chosen to highlight to changes in DS ratio and TTP throughout a single Lundberg B wave, where correlations to the invasive ICP signal are observed, as well as hemispheric variations.

## Early Diastolic/ Systolic Ratio (DS Ratio)

We used feature extraction to identify and calculate the DS ratio per cardiac cycle for the Day 4 recording period (Figure 1F), for the invasive ICP signal, left, and right brain optical signals. These calculated outputs in time are plotted as points in Figures 3A and B) with a rolling average line added for clarity.

By direct comparison of the DS ratios derived from the brain signals to the maximum invasive ICP reference values (Figure 1F, lower), we found significant, yet low, coefficients of determination $R^2$ (Figure 3C and D, "all" regression line). While this indicates a weak yet statistically significant relationship, the time dependence relative to the onset of the Lundberg B waves may have more intricate relational mechanisms.

The periods of Lundberg B wave onset and periods following their crest were manually labelled (green and peach regions, respectively) (Figure 3A and B). As can be seen in the time series, the left and right brain DS ratios followed the Lundberg B wave rise but fell slower than the value calculated from the ICP signal. This is reflected in a stronger linear relationship between Lundberg B waves and DS ratios during the green rising periods ($R^2$ = 0.48 left; 0.81 right; Figure 3C and D) compared to those in the post-rise periods ($R^2$ = 0.07 left; 0.20 right; Figure 3C and D). All linear relationships were $p < 0.001$, save for the left-side post-rise ($p = 0.006$). In every subset of the data ("all", "rising", "post-rise"), the left-side signal DS ratio was higher in value and less correlated than the response observed in the right brain signal (Figure 3C and D).

Notably, the $R^2$ = 0.81 for the rising periods in the right brain signal, exceeds that of the DS ratio calculated from the invasive ICP signal, $R^2$ = 0.73, when correlated with the maximum ICP values.

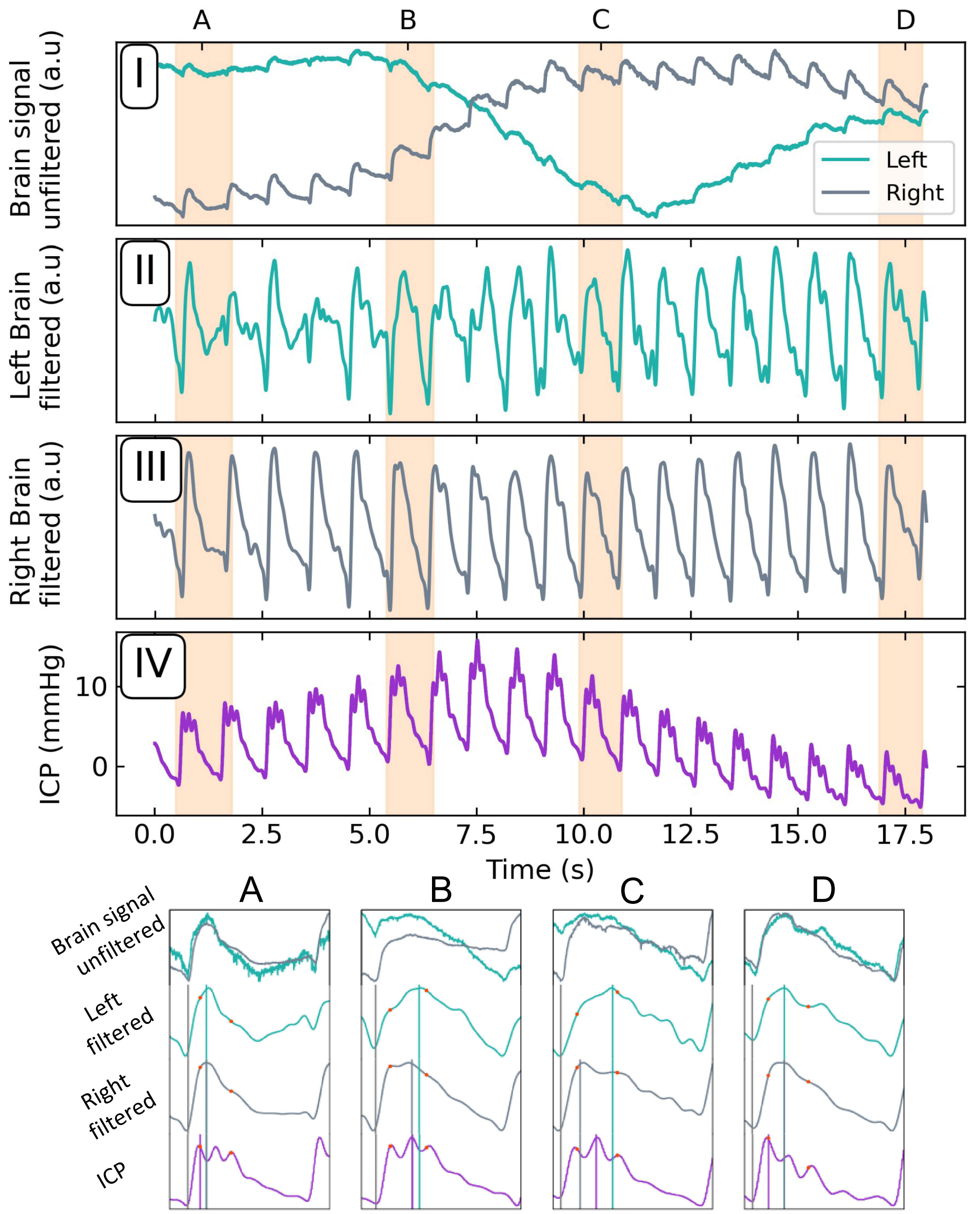


**Figure 2** Upper panels: (I) Unfiltered signals demonstrating the right and left-brain optical responses to a Lundberg B wave. Filtered left (II) and right (III) brain pulsatile component. (IV) Concurrent ICP recording of Lundberg B wave. Lower panel: Zoomed view of the periods (**A-D**) highlighted by the shaded areas of upper panels. Relative amplitudes at 45% and 10% of the pulse period (DS ratio) are marked with red dots; time to the pulse peak (TTP) by the vertical lines.
**Abbreviations**: a.u, arbitrary units; DS ratio, diastolic-systolic ratio; ICP, intracranial pressure mmHg, millimetres of mercury; sec, seconds.

## Time to Peak (TTP)

Figure 4 summarizes the equivalent analysis applied to the TTP values extracted from the three signals. The sharp transitions in the ICP TTP seen in Figure 4A) correspond to the Lundberg B waves and are due to the discrete shift from where P1 < P2 to P2 > P1 and back again. The transitions in the brain signals are less distinct owing to the less well-defined sub-peaks in the non-invasive signal.

The relationship between ICP and TTP is like that of the DS ratio analysis, though the difference between the right and left hemispheres is not as pronounced. The TTP rising onset showed the strongest relationship to ICP (right $R^2$ = 0.58; left $R^2$ = 0.44; both p < 0.001; Figure 4B and C), followed by the post-rise onset (right $R^2$ = 0.03, p = 0.078; left $R^2$ = 0.08, p = 0.002). When considering all data points together, the overall relationship between ICP and TTP is significantly weaker (right $R^2$ = 0.33, p = 0.078; left $R^2$ = 0.32, p = 0.002). Overall, these results demonstrate a linear relationship between invasive ICP and the TTP metric, though not as clear as that of the DS ratio.

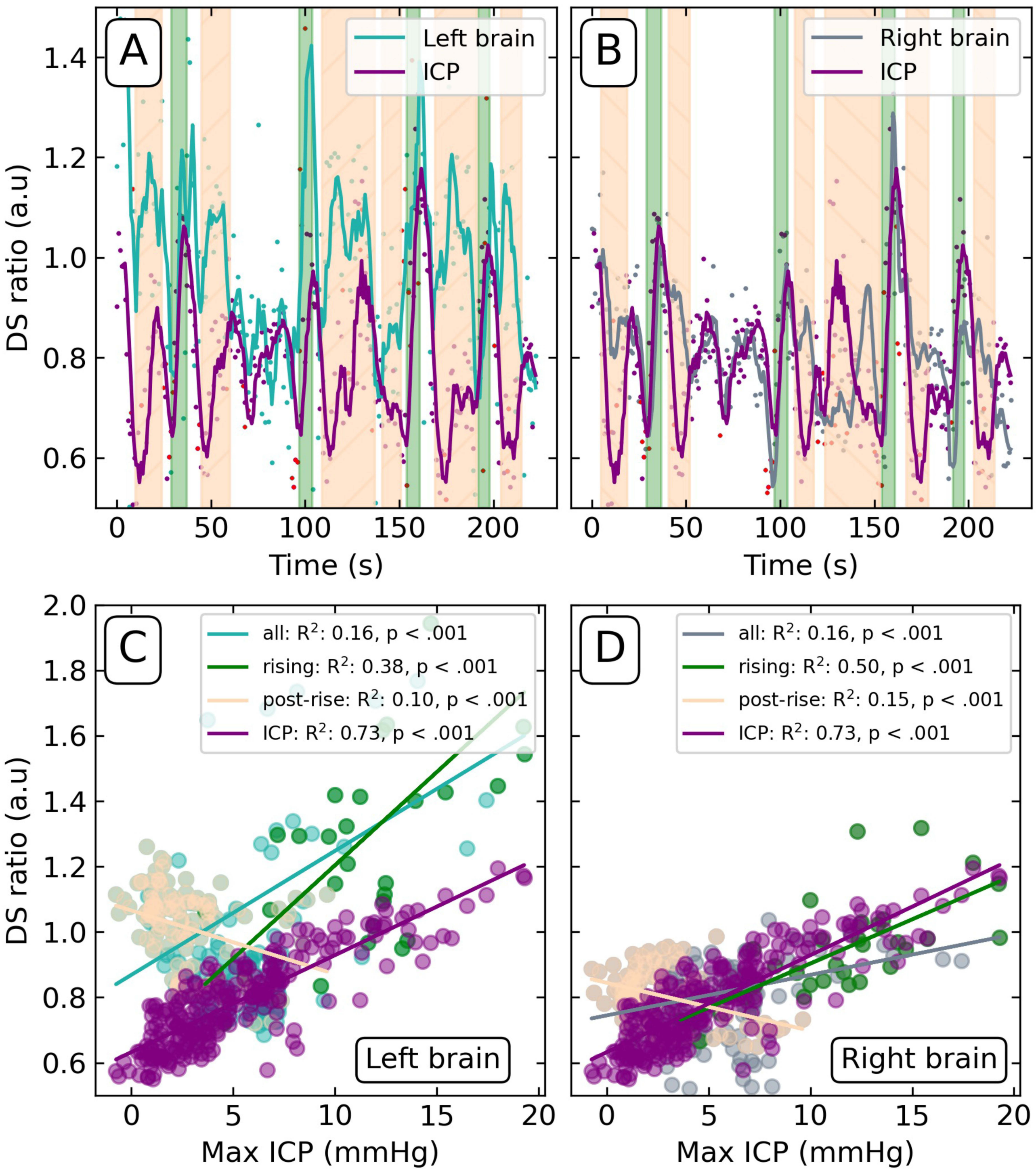


**Figure 3** DS ratio calculated for the ICP, left (**A**) and right (**B**) brain signals on Day 4. Green-shaded regions demarcate the rise of Lundberg B waves; peach-shaded regions demarcate post-rise periods. Red points denote values determined from periods of poor pulsatility signal. Scatter plots of the DS ratio of the left (**C**) and right (**D**) brain versus maximum invasive ICP levels. DS ratio of ICP correlated against maximum invasive ICP included for reference. Coefficient of determination ($R^2$) and p-value reported for all values ("all"), correlated green shaded regions of Lundberg B wave onset ("rising"), and anti-correlated periods following the waves ("post-rise").
**Abbreviations**: a.u, arbitrary units; DS ratio, diastolic-systolic ratio; ICP, intracranial pressure mmHg, millimetres of mercury; sec, seconds.

## Brain Oxygen ($StO_2$%) Levels

Brain tissue oxygen saturation also demonstrated slow oscillations ranging from 55 to 75% in both hemispheres (Figure 5A-C). The $R^2$ and p-values for the $StO_2$ returns compared to mean invasive ICP values were right $R^2 = 0.04$, $p < 0.001$; left $R^2 = 0.01$, $p = 0.005$, respectively (Figure 5D and E).

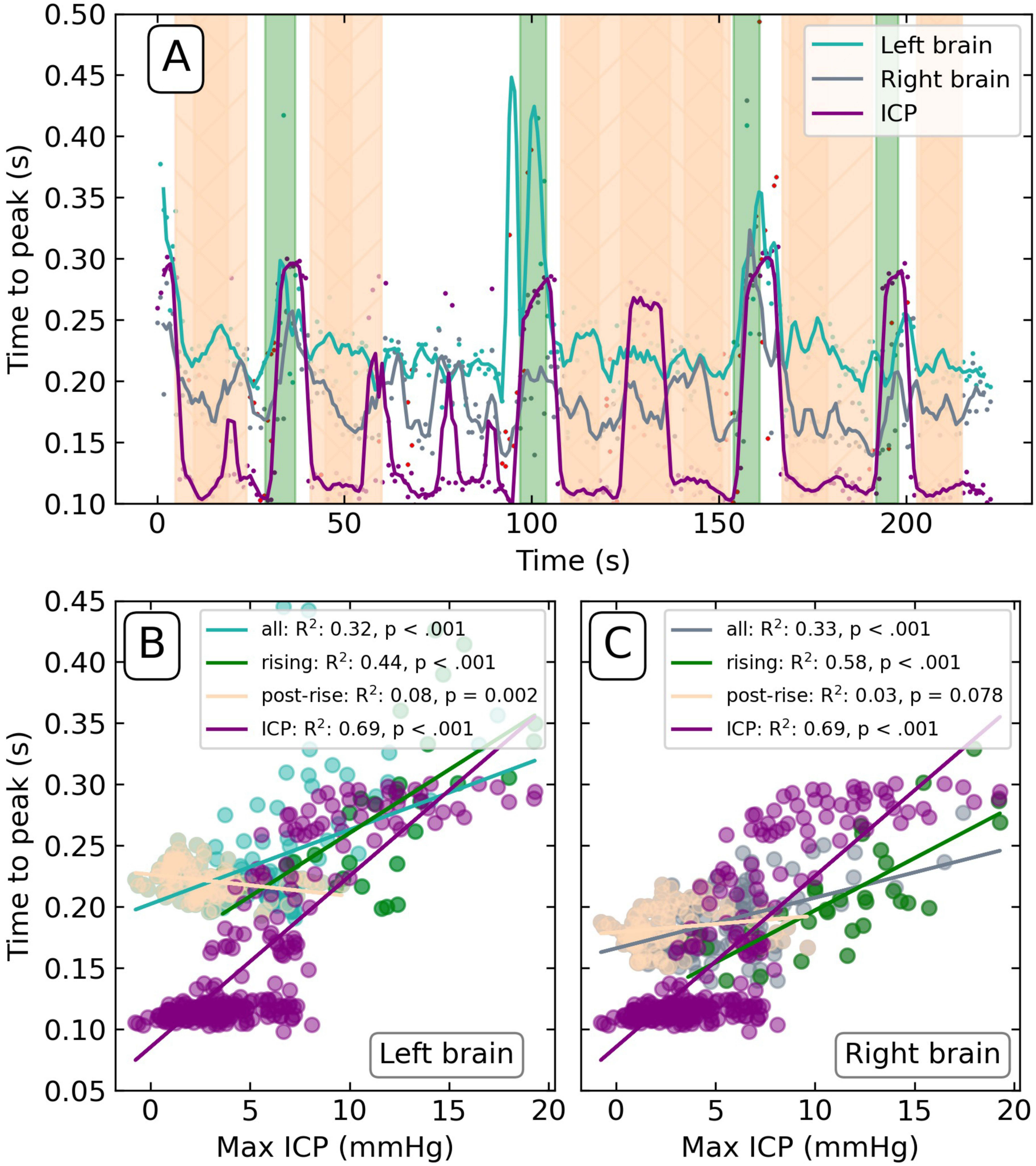


**Figure 4** (**A**) Time-to-peak (TTP) calculated from the invasive ICP, left and right brain signals on Day 4. Green-shaded regions demarcate the rise of Lundberg B waves; peach-shaded regions demarcate post-rise periods. Red points denote values determined from periods of poor pulsatility signal. Scatter plots of the TTP of left (**B**) and right (**C**) brain versus maximum invasive ICP levels. TTP of ICP correlated against maximum invasive ICP included for reference. Coefficient of determination ($R^2$) and p-value reported for all values ("all"), correlated green shaded regions of Lundberg B wave onset ("rising"), and anti-correlated periods following the waves ("post-rise").
**Abbreviations**: a.u, arbitrary units; DS ratio, diastolic-systolic ratio; ICP, intracranial pressure mmHg, millimetres of mercury; s, seconds; TTP, time-to-peak.

No linear relationship was observed between the right brain $StO_2$ values and Lundberg B waves (green regions). This is due to saturation of the 940nm wavelength optical intensity at these periods resulting in a lack of signal pulsatility, making it impossible to calculate an $StO_2$ value. This lack of valid data in these regions made a correlation analysis of rising onset of Lundberg B wave regions compared to all the data inconclusive.

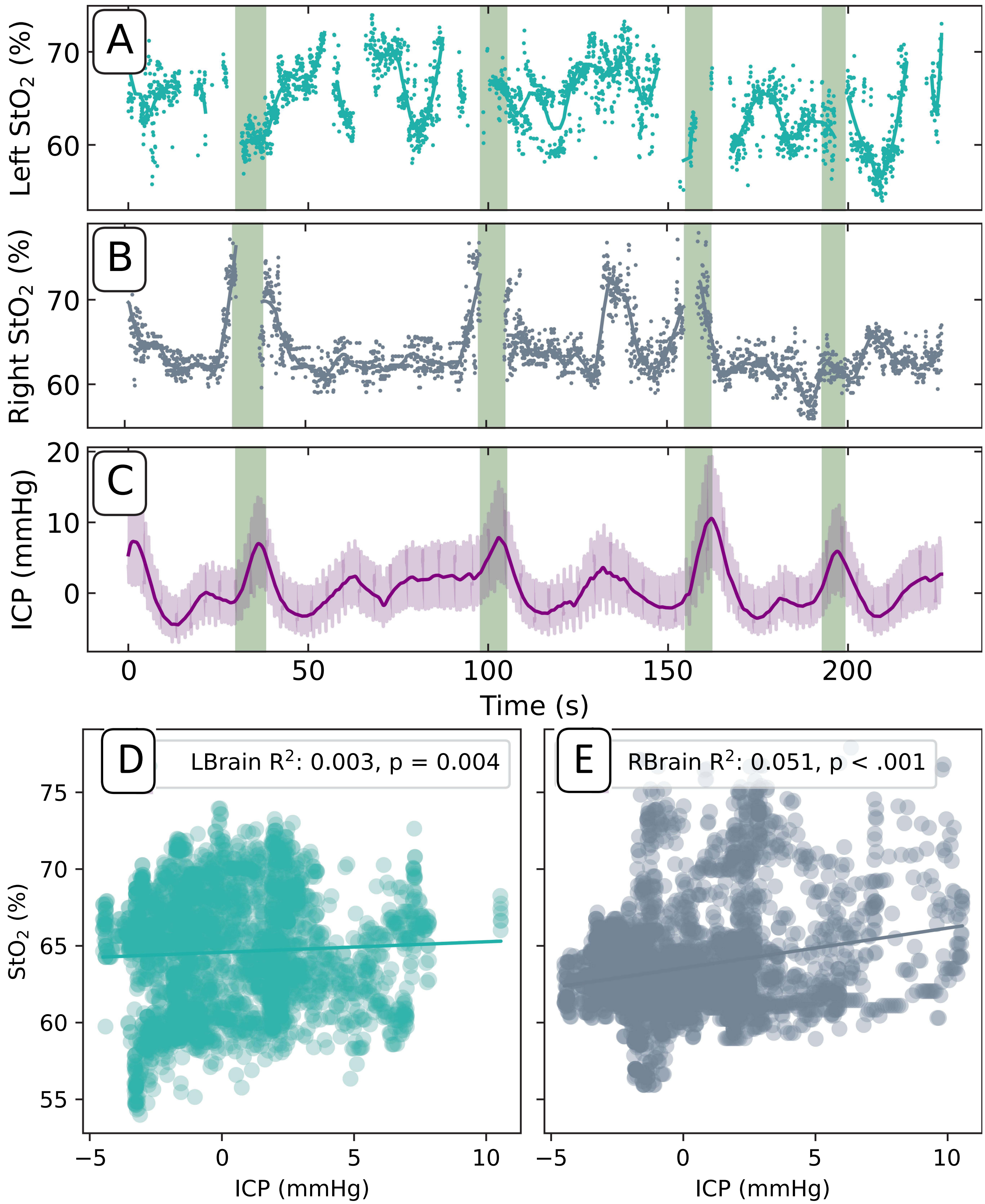


**Figure 5** Left (**A**) and right (**B**) brain pulse monitor tissue oxygen saturation levels ($StO_2$) on Day 4. (**C**) Invasive ICP (mean values, dark purple line) included for reference. Green shaded regions denote Lundberg B wave onsets. Scatter plots of the $StO_2$% and the maximum invasive ICP levels on the left (**D**) and the right (**E**). Coefficients of determination ($R^2$) and p-value are reported.

**Abbreviations**: a.u, arbitrary units; DS ratio, diastolic-systolic ratio; ICP, intracranial pressure; mmHg, millimetres of mercury; s, seconds; TTP, time-to-peak.

## Single Hemisphere Cardiac Pulsatility Attenuation

The right brain pulse waveform demonstrated intermittent brief episodes with a reduced or absent brain pulse (Figure 6A), lasting from 15 to 80 seconds. These episodes were frequently but not exclusively associated with the onset of Lundberg B waves (Figure 6F). Application of a Butterworth filter (3rd order, [0.5, 8.5] Hz) shows consistent cardiac pulsatility in the left-brain signal (Figure 6B) compared to that of the right (D). A continuous wavelet transform[39] was performed on the filtered data, further reinforcing the difference between the two sides. A threshold contour applied to the result shows a consistent band between 1 and 1.5 Hz for the left side (Figure 6C) compared to the right (Figure 6E), which has extremely spotty and inconsistent spectral power in the relevant band.

# Discussion

## Brain Compliance and ICP

The brain pulse waveform changes during the Lundberg B waves demonstrated features consistent with reduced compliance in both hemispheres, with an increase in the ratio of diastolic to early systolic pulse amplitudes (DS ratio) and a longer time to the pulse peak (TTP).[18,40–42]

Using these proxy indicators of brain compliance, we were able to demonstrate a significant linear relationship between the non-invasive monitor with the maximum invasive ICP values. The relationship between non-invasive ICP was most pronounced during the phase of the dominant ICP Lundberg B waves and showed a negative association immediately after the crest of the ICP spikes. These distinct behaviours may reflect the different physiological origins of the underlying signals and the anatomical location of the measurements. The invasive ICP is measured directly from the right lateral ventricle, while the brain pulse monitor's signal arises on the cortical surface from volume changes in the pial venous system associated with pulsatile brain expansion.

The consistent lead of DS ratio and TTP of the brain PPG relative to the rise in invasive ICP suggests that the brain PPG may more precisely reflect the compliance of the brain than the ICP alone.

## Oxygen Responses

We found a weak but significant temporal association on both the right and left-side $StO_2$ with the Lundberg B waves. The right-side slow oscillations were more clearly temporally associated than the left. The relationship between the Lundberg B waves and changes in brain oxygen is not well characterized. A large study using invasive $PbtO_2$ probes found little change in response to Lundberg B waves. The authors speculated that this may reflect the slow response time of the Licox $PbtO_2$ electrode.

The slow oscillations in oxygen in association with the ICP and brain compliance changes are consistent with the Lundberg B waves resulting from brief bilateral increases in cerebral blood flow in the MCA territories, as has been demonstrated in previous studies.[17] This compensatory response could be facilitated by an increase in cerebral blood flow or alterations in microvascular dynamics, such as a shift in the arteriole-venule ratio of blood. It has been previously shown that Lundberg B waves coincide with the dilation of pial arterioles.[20] Furthermore, an increase in ICP can compress and empty the pial venous system, thus reducing the blood volume.[28–31] These changes may enhance arterial inflow or enhance venous outflow resistance, thereby elevating $StO_2$ levels and driving elevated ICP. The precise underlying mechanisms, potentially involving changes in vascular tone or capillary recruitment, warrant further investigation to elucidate the relationship between ICP elevation and oxygen saturation, and how this interplay affects cerebral oxygenation status in the context of cerebral autoregulation.

Our findings that the left-brain signal showed higher compliance approximated by the DS ratio and TTP and brain oxygen oscillations, and less so with the Lundberg B waves, may indicate more injury within the left hemisphere. This is consistent with the clinical findings of weakness in the right leg and arm on discharge.

## Optical Intensity

The optical intensity demonstrated synchronous slow oscillations associated with the Lundberg B waves, with opposite hemispherical responses. We speculate that the origin of these phenomena could represent the movement of the brain.

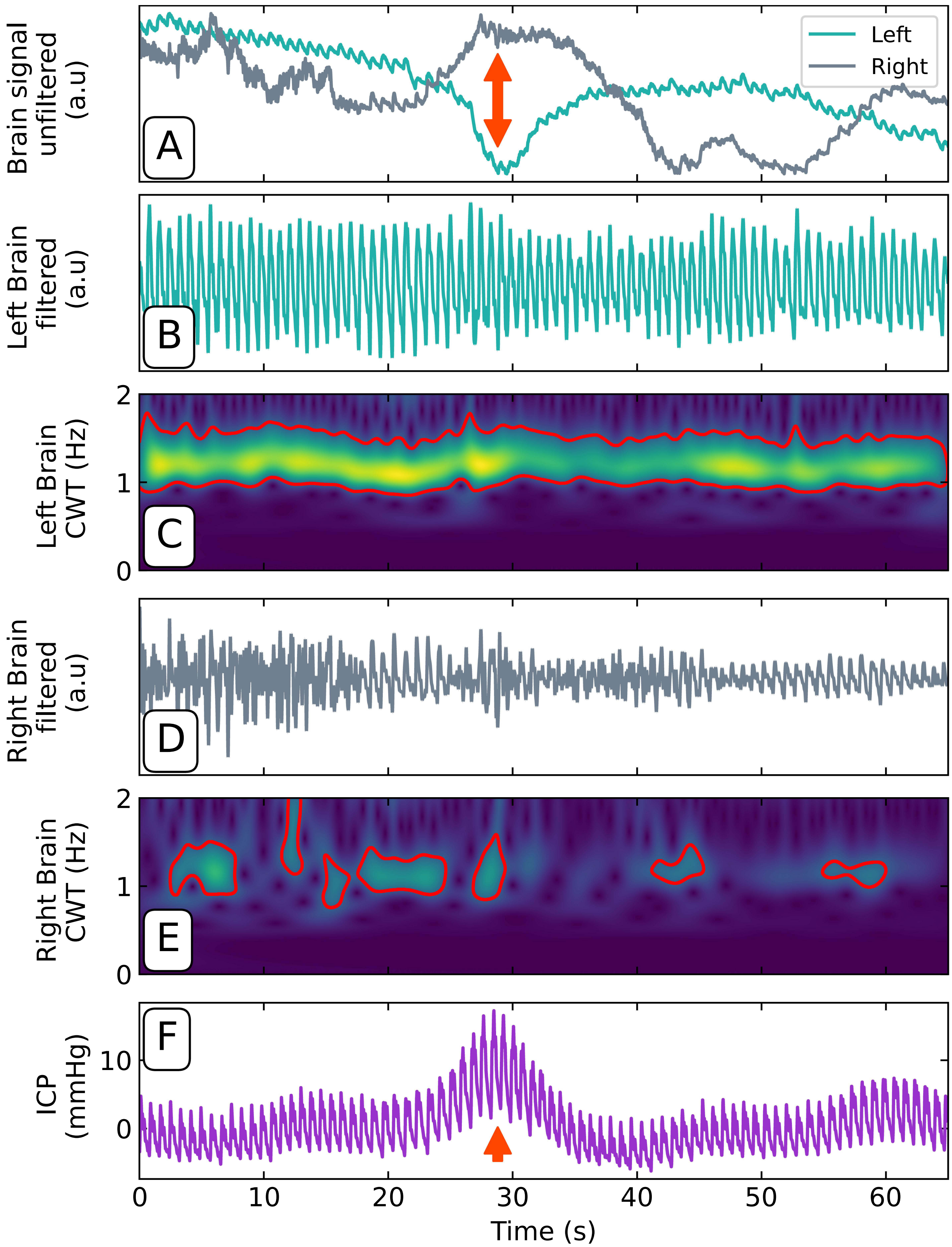


**Figure 6** (**A**) Unfiltered optical signals demonstrating the right and left brain responses to a Lundberg B wave (red arrow). Filtered left (**B**) and right (**D**) brain pulsatile component. Left (**C**) and right (**E**) brain continuous wavelet transformation (CWT) demonstrating the presence of a high amplitude left cardiac signal (yellow band, [1, 1.5] Hz) and absence (absent band) or reduced amplitude (green band) of the right cardiac signal. (**F**) Concurrent ICP recording of Lundberg B wave (red arrow).
**Abbreviations**: a.u, arbitrary units; CWT, continuous wavelet transform; DS ratio, diastolic-systolic ratio; Hz, hertz; ICP, intracranial pressure mmHg, millimetres of mercury; s, seconds.

Changes in cerebral blood flow and respiration may cause small but detectable movement of the brain lobes.[43–46] The position of the brain sensor over the temporal or frontal lobes may vary on the left and right sides and each lobe may have distinct movements. Brain injury can also influence the extent of brain movement.[47,48] Other potential factors include sub-arachnoid blood overlying the lobes and dynamic movement of CSF over the lobes in response to cerebral blood flow and respiration.[49,50] Other NIRS technologies, such as the NIRO 200, found similar slow oscillations in phase with Lundberg B waves. However, the direction of change was the same for both hemispheres.[51,52]

### Brief Episodes of Reduced or Absent Pulse on the Right Brain

The right brain signal demonstrated brief episodes of reduced or absent pulsatility. These lasted from 15 to 80 seconds and occurred in repeating cycles up to 2 times per minute. The onset typically occurred during the rising onset of a Lundberg B wave but also occurred at other times.

These observations could be interpreted as brief, but intense periods of reduced microvascular blood flow associated with vasoconstriction, as has been demonstrated in animal models of stroke and SAH.[5,53,54] Mechanisms include pial artery vasoconstriction triggered by spreading depolarization and pericyte constriction of capillaries.[5,55–57]

Some of the features in our case are consistent with spreading depolarization. In a peri-infarct animal model of spreading depolarization, ischemia triggered profound vasoconstriction lasting around 60 seconds with a gradual relaxation of vasoconstriction and return of blood flow.[55] These periods of microvascular vasoconstriction were associated with an increased risk of hypoxic injury.[55,58] A recent study found spikes in ICP also triggered spreading depolarization in an animal model, and similar responses were found in a series of patients with SAH.[59]

Other mechanisms could contribute to the loss of a cardiac signal including motion artefact associated with seizure or shivering causing fibrillation of the temporalis muscle that sits under the sensor, a similar artefact to what has been observed in EEG recordings.[60]

## Limitation

The findings presented here need to be interpreted with reasonable caution: the data presented originate from a single patient using a novel technology. During the period of monitoring blood pressure was not continuously assessed, a physiological measure we expect to enhance the interpretation of our observations. The brain signal can be influenced by movement artefacts such as shivering, swallowing or contraction of the temporalis muscles or other undetermined issues of mechanical origin. However, we do not believe these observations are associated with or can be explained by trivial external influences. As the technology is novel, further studies in other centres are required to provide greater clarity of the source and clinical significance of the brain pulse waveform changes presented here. We also have no gold standard comparator for our $StO_2\%$ calculations, so our estimations remain inferential and uncorroborated. The invasive ICP levels were generally within the normal range during these Lundberg B waves. Further assessment of the brain pulse monitor in patients with pathogenic ICP levels would be of value, as undertaken in our earlier study.[24]

## Conclusion

We assessed the cerebrovascular responses in a patient with Lundberg B waves following SAH, using a novel non-invasive brain monitor. The observed optical brain signals demonstrated slow oscillations in both hemispheres, synchronous with the Lundberg B waves identified from simultaneous invasive ICP measurements. The brain signal at the cardiac pulse level had waveform features qualitatively similar to raised ICP levels and reduced compliance during the Lundberg B waves, according to two metrics: an increase in the time to the pulse peak and an increase in the signal amplitude at the early diastolic phase relative to that at the early systolic phase. Brain oxygen levels derived from the optical signal also demonstrated slow oscillations associated with the Lundberg B waves.

These observations highlight the prospects for our non-invasive, optically based brain sensor to be a nuanced diagnostic tool, with its hemisphere-specific signal acquisition, responsive blood oxygen estimations, and derived features strongly correlated with the invasive ICP measurements.

## Ethics and Consent

This patient was enrolled as under the St Vincent's Hospital Melbourne Human Research Ethics Committee (HREC). Project ID Number: 63147. Approval received on 8th Sept 2020. Written informed consent for the publication of this case was provided by the next of kin.


## Acknowledgments

We would like to acknowledge Robert Tran from Keylead Health for his contributions to the algorithm development.


## Disclosure

B.D. is the founder and Chief Scientific Officer of Cyban, Pty Ltd and reports grants, personal fees from Cyban, during the conduct of the study; In addition, B.D. has patents US9717446B2 and WO2008134813A1 issued to Cyban. B.F., S.A. G., E.J.T., S.P., J.H. and J.S.S. are paid employees of Cyban. The hospital departments of P.S., A.J., and T.H. received financial support from Cyban to undertake the study. The authors report no other conflicts of interest in this work.

## References


1. Nakagawa M, Mutoh T, Takenaka S, et al. Asymptomatic Mild Hyperperfusion for the Prediction of Clinical Outcome in Postoperative Patients After Subarachnoid Hemorrhage. *Med Sci Monit*. 2017;23:285–291. doi:10.12659/MSM.899985
2. Terpolilli NA, Brem C, Bühler D, Plesnila N. Are We Barking Up the Wrong Vessels?: cerebral Microcirculation After Subarachnoid Hemorrhage. *Stroke*. 2015;46(10):3014–3019. doi:10.1161/STROKEAHA.115.006353
3. Dodd WS, Laurent D, Dumont AS, et al. Pathophysiology of Delayed Cerebral Ischemia After Subarachnoid Hemorrhage: a Review. *J Am Heart Assoc*. 2021;10(15):e021845. doi:10.1161/JAHA.121.021845
4. Dodd WS, Dayton O, Lucke-Wold B, Reitano C, Sorrentino Z, Busl KM. Decrease in cortical vein opacification predicts outcome after aneurysmal subarachnoid hemorrhage. *J Neurointerv Surg*. 2023;15(11):1105. doi:10.1136/jnis-2022-019578
5. Staehr C, Giblin JT, Gutiérrez-Jiménez E, et al. Neurovascular Uncoupling Is Linked to Microcirculatory Dysfunction in Regions Outside the Ischemic Core Following Ischemic Stroke. *J Am Heart Assoc*. 2023;12(11):e029527. doi:10.1161/JAHA.123.029527
6. Zhang Z, Fang Q, Zhang Y, et al. Magnetic resonance analysis of deep cerebral venous vasospasm after subarachnoid hemorrhage in rabbits. *Front Cardiovasc Med*. 2022;9:1013610. doi:10.3389/fcvm.2022.1013610
7. Friedrich B, Müller F, Feiler S, Schöller K, Plesnila N. Experimental Subarachnoid Hemorrhage Causes Early and Long-Lasting Microarterial Constriction and Microthrombosis: an *in-vivo* Microscopy Study. *J Cereb Blood Flow Metab*. 2012;32(3):447–455. doi:10.1038/jcbfm.2011.154
8. Vatter H, Güresir E, König R, et al. Invasive Diagnostic and Therapeutic Management of Cerebral VasoSpasm after Aneurysmal Subarachnoid Hemorrhage (IMCVS)—A Phase 2 Randomized Controlled Trial. *J Clin Med*. 2022;11(20):6197. doi:10.3390/jcm11206197
9. Alsbrook DL, Di Napoli M, Bhatia K, et al. Pathophysiology of Early Brain Injury and Its Association with Delayed Cerebral Ischemia in Aneurysmal Subarachnoid Hemorrhage: a Review of Current Literature. *J Clin Med*. 2023;12(3):1015. doi:10.3390/jcm12031015
10. McCredie VA, Chavarría J, Baker AJ. How do we identify the crashing traumatic brain injury patient – the intensivist's view. *Curr Opin Crit Care*. 2021;27(3):320–327. doi:10.1097/MCC.0000000000000825
11. Barone DG, Czosnyka M. Brain Monitoring: do We Need a Hole? An Update on Invasive and Noninvasive Brain Monitoring Modalities. *Sci World J*. 2014;2014:1–6. doi:10.1155/2014/795762
12. Stiefel MF, Spiotta A, Gracias VH, et al. Reduced mortality rate in patients with severe traumatic brain injury treated with brain tissue oxygen monitoring. *J Neurosurg*. 2005;103(5):805–811. doi:10.3171/jns.2005.103.5.0805
13. Svedung Wettervik T, Howells T, Hånell A, Ronne-Engström E, Lewén A, Enblad P. Low intracranial pressure variability is associated with delayed cerebral ischemia and unfavorable outcome in aneurysmal subarachnoid hemorrhage. *J Clin Monit Comput*. 2022;36(2):569–578. doi:10.1007/s10877-021-00688-y
14. Martinez-Tejada I, Arum A, Wilhjelm JE, Juhler M, Andresen M. B waves: a systematic review of terminology, characteristics, and analysis methods. *Fluids Barriers CNS*. 2019;16(1):33. doi:10.1186/s12987-019-0153-6
15. Lemaire JJ, Khalil T, Cervenansky F, et al. Slow Pressure Waves in the Cranial Enclosure. *Acta Neurochir (Wien)*. 2002;144(3):243–254. doi:10.1007/s007010200032
16. Balestreri M, Czosnyka M, Steiner LA, et al. Intracranial hypertension: what additional information can be derived from ICP waveform after head injury? *Acta Neurochir (Wien)*. 2004;146(2):131–141. doi:10.1007/s00701-003-0187-y
17. Newell DW, Nedergaard M, Aaslid R. Physiological Mechanisms and Significance of Intracranial B Waves. *Front Neurol*. 2022;13:872701. doi:10.3389/fneur.2022.872701
18. Lewis PM, Smielewski P, Rosenfeld JV, Pickard JD, Czosnyka M. A Continuous Correlation Between Intracranial Pressure and Cerebral Blood Flow Velocity Reflects Cerebral Autoregulation Impairment During Intracranial Pressure Plateau Waves. *Neurocrit Care*. 2014;21(3):514–525. doi:10.1007/s12028-014-9994-7
19. Spiegelberg A, Preuß M, Kurtcuoglu V. B-waves revisited. *Interdiscip Neurosurg*. 2016;6:13–17. doi:10.1016/j.inat.2016.03.004
20. Auer LM, Sayama I. Intracranial pressure oscillations (B-waves) caused by oscillations in cerebrovascular volume. *Acta Neurochir (Wien)*. 1983;68(1):93–100. doi:10.1007/BF01406205
21. Lescot T, Naccache L, Bonnet MP, Abdennour L, Coriat P, Puybasset L. The relationship of intracranial pressure Lundberg waves to electroencephalograph fluctuations in patients with severe head trauma. *Acta Neurochir (Wien)*. 2005;147(2):125–129. doi:10.1007/s00701-004-0355-8
22. Dixon B, MacLeod DB. Assessment of a Non Invasive Brain Oximeter in Volunteers Undergoing Acute Hypoxia. *Med Devices Evidence Res*. 2020;13:183–194. doi:10.2147/MDER.S250102

23. Dixon B, Turner R, Christou C. Assessment of a Non-Invasive Brain Oximeter in a Sheep Model of Acute Brain Injury. *Med Devices Evidence Res*. 2019;12:479–487. doi:10.2147/MDER.S235804
24. Dixon B, Sharkey JM, Teo EJ, et al. Assessment of a Non-Invasive Brain Pulse Monitor to Measure Intra-Cranial Pressure Following Acute Brain Injury. *Med Devices Evidence Res*. 2023;16:15–26. doi:10.2147/MDER.S398193
25. Kyriacou PA. *Photoplethysmography: Technology, Signal Analysis and Applications*. Elsevier, AP Academic Press; 2022.
26. Gopinath SP, Robertson CS, Contant CF, Narayan RK, Grossman RG, Chance B. Early detection of delayed traumatic intracranial hematomas using near-infrared spectroscopy. *J Neurosurg*. 1995;83(3):438–444. doi:10.3171/jns.1995.83.3.0438
27. ROBERTSON CS, GOPINATH SP, CHANCE B. A New Application for Near-Infrared Spectroscopy: detection of Delayed Intracranial Hematomas after Head Injury. *J Neurotrauma*. 1995;12(4):591–600. doi:10.1089/neu.1995.12.591
28. Unnerbäck M, Ottesen JT, Reinstrup P. ICP curve morphology and intracranial flow-volume changes: a simultaneous ICP and cine phase contrast MRI study in humans. *Acta Neurochir (Wien)*. 2018;160(2):219–224. doi:10.1007/s00701-017-3435-2
29. Unnerbäck M, Ottesen JT, Reinstrup P. Increased Intracranial Pressure Attenuates the Pulsating Component of Cerebral Venous Outflow. *Neurocrit Care*. 2019;31(2):273–279. doi:10.1007/s12028-019-00733-4
30. Greitz D, Wirestam R, Franck A, Nordell B, Thomsen C, Ståhlberg F. Pulsatile brain movement and associated hydrodynamics studied by magnetic resonance phase imaging. *Neuroradiology*. 1992;34(5):370–380. doi:10.1007/BF00596493
31. Nakagawa Y, Tsuru M, Yada K. Site and mechanism for compression of the venous system during experimental intracranial hypertension. *J Neurosurg*. 1974;41(4):427–434. doi:10.3171/jns.1974.41.4.0427
32. Harris CR, Millman KJ, Van Der Walt SJ, et al. Array programming with NumPy. *Nature*. 2020;585(7825):357–362. doi:10.1038/s41586-020-2649-2
33. Virtanen P, Gommers R, Oliphant TE, et al. SciPy 1.0: fundamental algorithms for scientific computing in Python. *Nat Methods*. 2020;17(3):261–272. doi:10.1038/s41592-019-0686-2
34. Brasil S. Intracranial pressure pulse morphology: the missing link? *Intensive Care Med*. 2022;48(11):1667–1669. doi:10.1007/s00134-022-06855-2
35. Aspide R, Moneti M, Castioni CA. Are Intracranial Pressure Waveforms the New Frontier for Noninvasive Assessment of Intracranial Pressure? *Neurocrit Care*. 2023;s12028-023-01785–3. doi:10.1007/s12028-023-01785-3
36. Brasil S, Godoy DA, Hawryluk GWJ. A Point-of-Care Noninvasive Technique for Surrogate ICP Waveforms Application in Neurocritical Care. *Neurocrit Care*. 2023. doi:10.1007/s12028-023-01786-2
37. Wang H, Siu K, Ju K, Chon KH. A High Resolution Approach to Estimating Time-Frequency Spectra and Their Amplitudes. *Ann Biomed Eng*. 2006;34(2):326–338. doi:10.1007/s10439-005-9035-y
38. Bashar SK, Han D, Hajeb-Mohammadalipour S, et al. Atrial Fibrillation Detection from Wrist Photoplethysmography Signals Using Smartwatches. *Sci Rep*. 2019;9(1):15054. doi:10.1038/s41598-019-49092-2
39. Mallat S. *A Wavelet Tour of Signal Processing*. Second. Elsevier; 1999.
40. Brasil S, Solla DJF, Nogueira RDC, Jacobsen Teixeira M, Malbouisson LMS, Paiva WS. Intracranial Compliance Assessed by Intracranial Pressure Pulse Waveform. *Brain Sci*. 2021;11(8):971. doi:10.3390/brainsci11080971
41. Smits M, Dippel DWJ, Steyerberg EW, et al. Predicting Intracranial Traumatic Findings on Computed Tomography in Patients with Minor Head Injury: the CHIP Prediction Rule. *Ann Intern Med*. 2007;146(6):397–405. doi:10.7326/0003-4819-146-6-200703200-00004
42. Ellis T, McNames J, Aboy M. Pulse Morphology Visualization and Analysis With Applications in Cardiovascular Pressure Signals. *IEEE Trans Biomed Eng*. 2007;54(9):1552–1559. doi:10.1109/TBME.2007.892918
43. Hermes D, Wu H, Kerr AB, Wandell BA. Measuring brain beats: cardiac-aligned fast functional magnetic resonance imaging signals. *Hum Brain Mapp*. 2023;44(1):280–294. doi:10.1002/hbm.26128
44. Britt RH, Rossi GT. Quantitative analysis of methods for reducing physiological brain pulsations. *J Neurosci Methods*. 1982;6(3):219–229. doi:10.1016/0165-0270(82)90085-1
45. Wilson MH. Monro-Kellie 2.0: the dynamic vascular and venous pathophysiological components of intracranial pressure. *J Cereb Blood Flow Metab*. 2016;36(8):1338–1350. doi:10.1177/0271678X16648711
46. Terem I, Ni WW, Goubran M, et al. Revealing sub-voxel motions of brain tissue using phase-based amplified MRI (aMRI). *Magn Reson Med*. 2018;80(6):2549–2559. doi:10.1002/mrm.27236
47. Smith WS, Browne JL, Ko NU. Cranial Accelerometry Can Detect Cerebral Vasospasm Caused by Subarachnoid Hemorrhage. *Neurocrit Care*. 2015;23(3):364–369. doi:10.1007/s12028-015-0118-9
48. Smith WS, Keenan KJ, Lovoi PA. A Unique Signature of Cardiac-Induced Cranial Forces During Acute Large Vessel Stroke and Development of a Predictive Model. *Neurocrit Care*. 2020;33(1):58–63. doi:10.1007/s12028-019-00845-x
49. SAKAKIBARA Y, YATSUSHIRO S, Konta N, HORIE T, KURODA K, MATSUMAE M. Respiratory-driven Cyclic Cerebrospinal Fluid Motion in the Intracranial Cavity on Magnetic Resonance Imaging: insights into the Pathophysiology of Neurofluid Dysfunction. *Neurol Med Chir (Tokyo)*. 2021;61(12):711–720. doi:10.2176/nmc.oa.2021-0160
50. Taoka T, Kawai H, Nakane T, et al. Evaluating the Effect of Arterial Pulsation on Cerebrospinal Fluid Motion in the Sylvian Fissure of Patients with Middle Cerebral Artery Occlusion Using Low b-value Diffusion-weighted Imaging. *Magn Reson Med Sci*. 2021;20(4):371–377. doi:10.2463/mrms.mp.2020-0121
51. Weerakkody RA, Czosnyka M, Zweifel C, et al. Slow vasogenic fluctuations of intracranial pressure and cerebral near infrared spectroscopy—an observational study. *Acta Neurochir (Wien)*. 2010;152(10):1763–1769. doi:10.1007/s00701-010-0748-9
52. Diedler J, Zweifel C, Budohoski KP, et al. The Limitations of Near-Infrared Spectroscopy to Assess Cerebrovascular Reactivity: the Role of Slow Frequency Oscillations. *Anesth Analg*. 2011;113(4):849–857. doi:10.1213/ANE.0b013e3182285dc0
53. Mei YX, Hao CX, fei LJ, man ZC, yan HJ, Hua CC. In vivo observation of cerebral microcirculation after experimental subarachnoid hemorrhage in mice. *Neural Regen Res*. 2018;13(3):456. doi:10.4103/1673-5374.228728
54. O'Herron PJ, Hartmann DA, Xie K, Kara P, Shih AY. 3D optogenetic control of arteriole diameter in vivo. *eLife*. 2022;11:e72802. doi:10.7554/eLife.72802
55. Shin HK, Dunn AK, Jones PB, Boas DA, Moskowitz MA, Ayata C. Vasoconstrictive Neurovascular Coupling during Focal Ischemic Depolarizations. *J Cereb Blood Flow Metab*. 2006;26(8):1018–1030. doi:10.1038/sj.jcbfm.9600252

56. Tran CHT, George AG, Teskey GC, Gordon GR. Seizures elevate gliovascular unit Ca2+ and cause sustained vasoconstriction. *JCI Insight*. 2020;5(19):e136469. doi:10.1172/jci.insight.136469
57. Freischmidt A, Wieland T, Richter B, et al. Haploinsufficiency of TBK1 causes familial ALS and fronto-temporal dementia. *Nat Neurosci*. 2015;18(5):631–636. doi:10.1038/nn.4000
58. Kirchner T, Gröhl J, Herrera MA, et al. Photoacoustics can image spreading depolarization deep in gyrencephalic brain. *Sci Rep*. 2019;9(1):8661. doi:10.1038/s41598-019-44935-4
59. Oka F, Sadeghian H, Yaseen MA, et al. Intracranial pressure spikes trigger spreading depolarizations. *Brain*. 2022;145(1):194–207. doi:10.1093/brain/awab256
60. Yilmaz G, Ungan P, Sebik O. Interference of tonic muscle activity on the EEG: a single motor unit study. *Front Hum Neurosci*. 2014;8. doi:10.3389/fnhum.2014.00504